

Auto-selection of quasi-components/components in the multi-dimensional quasi-discrete model

Mansour Al Qubeissi^{1,2*}, Nawar Al-Esawi^{1,3}, Sergei S. Sazhin⁴

¹*Institute for Future Transport and Cities, Coventry University, Coventry CV1 5FB, United Kingdom*

²*Faculty of Engineering, Environment and Computing, Coventry University, Coventry CV1 2JH, United Kingdom*

³*Faculty of Arts, Science and Technology, University of Northampton, Northampton, NN1 5PH, United Kingdom*

⁴*Advanced Engineering Centre, University of Brighton, Brighton BN2 4GJ, United Kingdom*

1 Abstract

2 A new algorithm for the auto-selection of quasi-components and components (QC/Cs) in the
3 'multi-dimensional quasi-discrete' model is suggested. This algorithm is applied to the
4 analysis of heating and evaporation of multi-component fuel droplets. It allows one to
5 automatically select QC/Cs and update the initial selection during droplet evaporation. The
6 new algorithm is expected to be applicable to the analysis of a wide range of fuels and fuel
7 blends. It can be directly implemented into CFD codes with minimal intervention by end-
8 user. Using this algorithm, the effects of transient diffusion of species on droplet lifetimes are
9 investigated for mixtures of Diesel and E85 (85% vol. ethanol and 15% vol. gasoline) fuels.
10 It is shown that the new algorithm can reduce the analysis of the E85-Diesel fuel droplets,
11 taking into account the contributions of up to 119 components at the initial stage of heating
12 and evaporation, to that based on 5 QC/Cs, near the end of droplet evaporation, with up to
13 1.9% errors in predicted droplet temperatures and radii. The CPU time needed to perform
14 calculations using the new algorithm is shown to be 80% less than that when considering
15 the full composition of fuel.

16 **Keywords:** Auto-selection algorithm; Evaporation; Fuel blends; Heating; Multi-component
17 fuels; Quasi-components

18 Nomenclature

19 Abbreviations

CFD	Computational Fluid Dynamics
CFS	Complex Fuel Surrogates
CPU	Central Processing Unit (in computers)
DC	Discrete Component (model)
E85	Fuel mixture of 85% ethanol and 15% gasoline (volume fraction)
ED	Effective Diffusivity

* Corresponding author: Telephone: +44-(0)2477-658060, E-mail: Mansour.Qubeissi@coventry.ac.uk

ETC	Effective Thermal Conductivity
FACE	Fuel used in Advanced Combustion Engines
MDQD	Multi-Dimensional Quasi-Discrete (model)
QC/Cs	Quasi-Components/ Components
TMDQD	Transient Multi-Dimensional Quasi-Discrete (algorithm)
T.S.	Time Saving
UNIFAC	Universal Quasi-Chemical Functional-group Activity Coefficient

20 Mathematical Scripts

Symbol	Definition	Units
B_M	Spalding mass transfer number	-
c	Specific heat capacity	$\text{J}\cdot\text{kg}^{-1}\text{K}^{-1}$
D	Diffusion coefficient	m^2s^{-1}
d_o	Droplet initial diameter	m (or μm)
G	Group mass fraction	-
h	Convective heat transfer coefficient	$\text{W}\cdot\text{m}^{-2}\text{K}^{-1}$
F	Reduction factor in the number of components	-
K	Minimum change in the ratio of group mass fractions	-
k	Thermal conductivity	$\text{W}\cdot\text{m}^{-1}\text{K}^{-1}$
L	Latent heat of evaporation	$\text{J}\cdot\text{kg}^{-1}$
\dot{m}	Evaporation rate of droplets	$\text{kg}\cdot\text{s}^{-1}$
n	Carbon number	-
N	Number of species	-
Nu	Nusselt number	-
p	Pressure	Pa
p^*	Saturated pressure	Pa
Pr	Prandtl number	-
Pe	Peclet number	-
R	Distance from the droplet centre	m (or μm)
\dot{R}_d	Rate of change in droplet radius	$\text{m}\cdot\text{s}^{-1}$
Re	Reynolds number	-
Sc	Schmidt number	-
t	Time	s (or ms)
T	Temperature	K
U	Velocity	$\text{m}\cdot\text{s}^{-1}$
$v_n; v_{nY}$	Eigenfunctions used in Expressions (7), (10) and (11)	-
X	Molar fraction	-
Y	Mass fraction	-

21 Subscripts

d	Droplet
e	Change due to evaporation
eff	Effective

g	Gas
i	Index of species or their chemical groups
iso	Isolated
j	Index of species forming quasi-components
k	Index of the newly formed QC/Cs
l	Liquid or the numbers of components that form each QC/C (Exprs. (1) and 2))
s	Surface of the droplet
v	Vapour
∞	Far from the droplet surface

22 **Greek Scripts**

γ	Activity coefficient	-
ϵ	Relative evaporation rate	-
ε	Minimum ratio of droplet radii	-
κ_R	Effective thermal diffusivity divided by R_d^2	s^{-1}
λ	Eigenvalues in Expressions (7) and (9)	-
μ	Dynamic viscosity	Pa·s
ρ	Density	$kg \cdot m^{-3}$
χ	Correction factors in Expressions (8) and (12)	-
Δ	Relative change	-

23 **1. Introduction**

24 Spray combustion is a complex process, involving two-phase flow, heat and mass transfer in multi-
 25 component fuels, and chemical reactions [1,2]. Fuel spray formation in a combustion chamber
 26 includes jet break-up into small droplets to form an air-fuel mixture and heating and evaporation of
 27 these small droplets. The modelling of these processes is computationally expensive, and not possible
 28 without simplification [3]. This difficulty increases when realistic compositions of fuels and their
 29 blends, containing hundreds of components, need to be taken into account [4]. Therefore, it is
 30 necessary to consider the computational efficiency when developing these models to achieve a
 31 balance between computational expense and model accuracy. The treatment of sprays as an array of
 32 a large number of spherical droplets is widely accepted [5]. Thus, the analysis of evaporation of
 33 sprays can be focused on the analysis of evaporation of isolated individual droplets.

34 Fuel droplet heating and evaporation are essential thermophysical processes in many engineering
 35 applications, including automotive systems [5]. The importance of modelling of these processes has
 36 been discussed in many papers (e.g. [6–9]). Fuel droplets, used in engineering applications, are
 37 typically complex mixtures of various chemical groups [10]. These groups and their properties need
 38 to be considered carefully for accurate simulation of droplet heating and evaporation [11–13].
 39 However, when all fuel components are accounted for (e.g. using the Discrete Component (DC)
 40 model; see [14–17] for the details), calculations are likely to be computationally expensive [18]. This
 41 problem has been addressed by replacing large numbers of components in fuels with much smaller

42 numbers of representative components, referred to as ‘quasi-components and components’ (QC/Cs),
43 in the relatively simple ‘quasi-discrete’ model [19] and its more advanced version, the ‘multi-
44 dimensional quasi-discrete’ (MDQD) model [4].

45 The MDQD model focuses on the analysis of quasi-components (fictitious components with non-
46 integer numbers of atoms) rather than on the actual components used in the DC model. The MDQD
47 model was applied to the analysis of heating and evaporation of droplets of Diesel and gasoline fuels,
48 and their blends with biodiesel and ethanol [4,20–24], and showed substantial improvement in
49 computational efficiency with only a small loss of accuracy. As quasi-components (QCs) used in this
50 model have non-integer carbon numbers, in the general case, their combustion characteristics cannot
51 be described. Also, the choice of QCs in the original version of this model was based on the trial-and
52 error-approach, which made it difficult to implement it into CFD codes. In our most recent study [25],
53 the number of fuel components was reduced via the introduction of representative components using
54 the so-called approximate nearest-integer discrete method. This led to the formulation of Complex
55 Fuel Surrogates (CFS) which were found to be useful in the combustion simulation. As in the original
56 MDQD model, however, the selection of representative components in the CFS model was based on
57 the trial-and-error approach.

58 This paper focuses on further development of the MDQD model by introducing a new algorithm
59 for automatic selection of quasi-components/components (QC/Cs) during the droplet evaporation
60 process (called TMDQD, where T stands for transient). In the following section, this new algorithm is
61 described. The basic equations of droplet heating and evaporation, used in our analysis, are briefly
62 described in Section 3. The fuel compositions are presented in Section 4. The results of application of
63 the new algorithm to typical fuel droplets are presented in Section 5. In Section 6, the main findings
64 are summarised.

65 2. Selection algorithm

66 In the MDQD model, realistic fuel compositions are reduced to a smaller number of quasi-
67 components/components (QC/Cs), with carbon numbers averaged over the groups of individual
68 components with close carbon numbers [4]. In most case, this averaging leads to non-integer carbon
69 numbers, something which is not possible for actual components. These new structures with non-
70 integer carbon numbers are called ‘quasi-components’. These quasi-components are treated
71 similarly to the actual components with thermodynamic and transport properties interpolated
72 between those of the components with the nearest integer carbon numbers. For each group of
73 components i (in the case of Diesel fuel, there are 9 such hydrocarbon groups), the carbon numbers
74 of the quasi-components/components (QC/Cs) are calculated as:

$$n_{k_i} = \frac{\sum_{j=j}^{j=J+\ell_{ij}} (n_j X_j)}{\sum_{j=j}^{j=J+\ell_{ij}} X_j} \quad (1)$$

75 where ℓ_{ij} are the numbers of components that form each QC/C in group i , for a given value of J ; j is
 76 the index of the species forming each QC/C in group i in the range J to $J + \ell_{ij}$, and k_i is the index of
 77 the QC/Cs in group i . The numbers ℓ_{ij} are predefined by the end-user at the initial stage of
 78 calculation, based on the initial distribution of species; they do not change during the evaporation
 79 process unless species are completely evaporated. The molar fractions of species that form certain
 80 QC/Cs are summed up to calculate the molar fractions of those QC/Cs, as follows:

$$X_{k_i} = \sum_{j=J}^{j=J+\ell_{ij}} X_j, \quad (2)$$

81 where subscript ' k_i ' refers to a specific QC/C in group i .

82 In contrast to the original application of the MDQD model, the new algorithm does not require
 83 direct user involvement in the selection of QC/Cs. Changes in the number of QC/Cs are allowed during
 84 the process of droplet heating and evaporation. A flowchart for the new algorithm is shown in Figure
 85 1. Initially ($t=0$), the number of components is taken equal to the total number of components (i.e.
 86 the DC model is used for the prediction of droplet heating and evaporation). Then, during the
 87 evaporation process, the formation of QC/Cs is allowed within each group of hydrocarbons, as in the
 88 conventional MDQD model. In contrast to the conventional MDQD model, the number of QC/Cs within
 89 each group is not pre-selected by the user but is determined by the code at each time-step.

90 The new algorithm allows automatic reduction of the number of QC/Cs from their initial number
 91 to a smaller number, which is determined by the algorithm at specific time-steps. The mass fraction
 92 of group i at a certain time-step (G_i) increases or decreases compared with its value in the previous
 93 time-step ($G_{i_{old}}$). The species mass fractions are more sensitive to transient effects than their molar
 94 fractions; hence, their use in this model to calculate G_i :

$$G_i = \sum_{n=1}^{N_i} Y_{ni}, \quad (3)$$

95 where Y_{ni} are the mass fractions of individual species n in group i and N_i is the total number of species
 96 in the same group i (in the case of Diesel fuel, $N_i \leq 20$ for all groups). The change in G_i is estimated
 97 as:

$$\Delta G_i = \frac{|G_i - G_{i_{old}}|}{G_i}, \quad (4)$$

98 If ΔG_i is greater than an *a priori* chosen small number K (in our current analysis, $K = 0.1$), the
 99 number of QC/Cs within each group (N_i) is reduced from the previous number ($N_{i_{old}}$) by a certain
 100 factor F :

$$N_i = [F N_{i_{old}}], \quad (5)$$

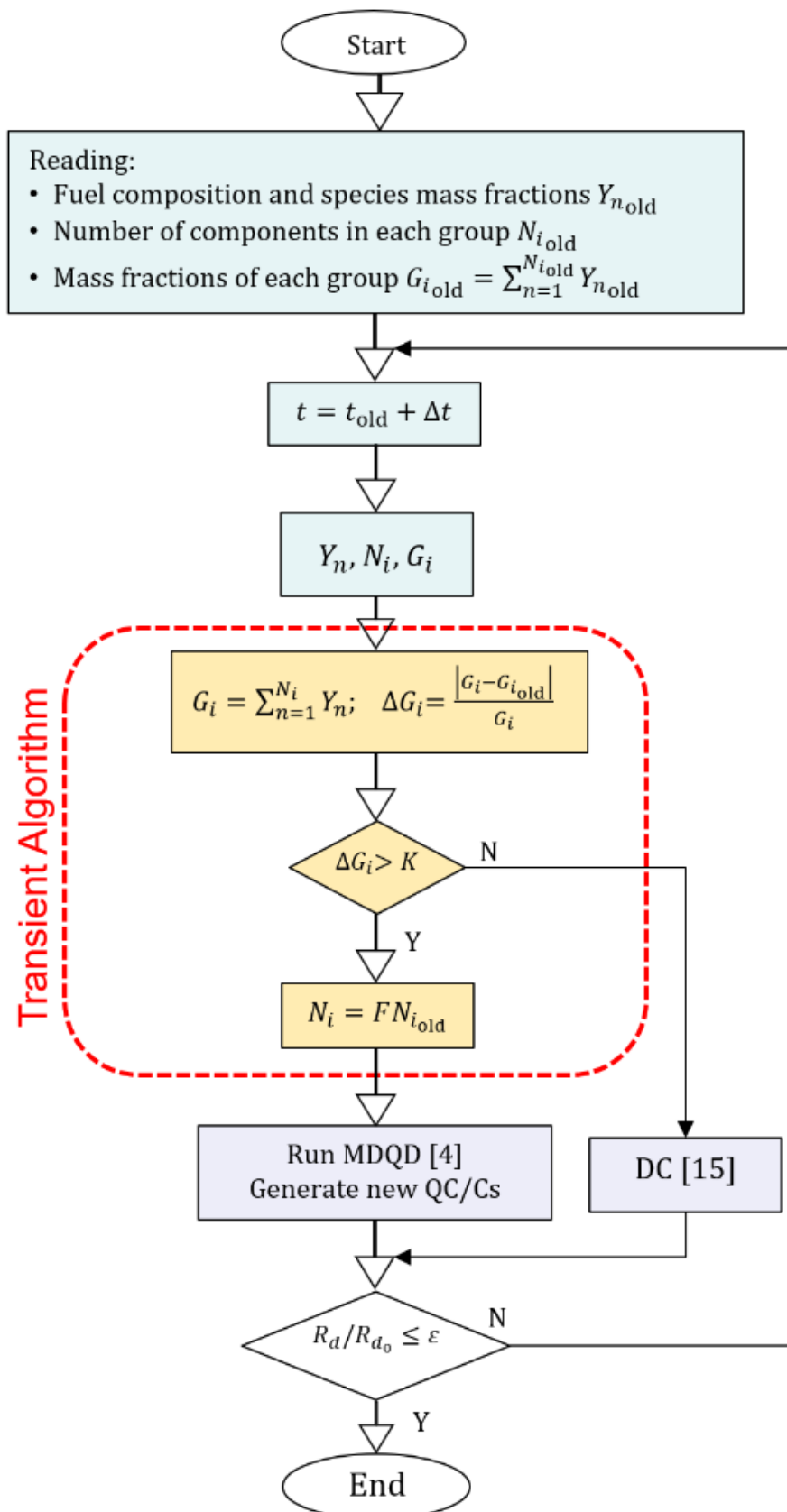
101 where F is assumed equal to 0.75, $[\]$ indicates rounding up or down to the nearest integer (e.g.
 102 $[7.5]=8$ and $[7.4]=7$). The number 0.75 is proposed, using a trial-and-error approach, to avoid rapid

103 reduction in the numbers of QC/Qs at the expense of accuracy for lower F or slow reduction in the
 104 numbers of QC/Qs at the expense of computational speed for higher F .

105 The QCs in our algorithm are formed of the components with the smallest molar fractions in any
 106 group i . The selection is based on reverse collation of components to accommodate merging the least
 107 contributing components in that group first, starting with the components with the largest carbon
 108 numbers (usually the smallest molar fractions) and ending up with the components with the smallest
 109 carbon numbers, and usually the highest molar contributions. The number of QC/Cs selected to form
 110 the new QCs is taken equal to $\lceil N_i/2 \rceil$. In the case where $\lceil N_i/2 \rceil$ is an even number, the QCs are formed
 111 of each 2 components in the half of components with the largest carbon numbers. If $\lceil N_i/2 \rceil$ is an odd
 112 number, however, then the nearest component that is not selected is added to this group to form an
 113 even number of components and each two QC/Cs in this group are merged to form a new QC. For
 114 example, in the case of the alkanes, which include 20 of 98 Diesel fuel components, at the initial stage
 115 ($N_{i_{old}} = 20$), $N_i = \lceil 0.75 \times 20 \rceil = 15$ QC/Cs after the first reduction of the number of components.
 116 The first 10 components remain unchanged, and the remaining 10 components form 5 QCs (each 2
 117 components form 1 QC). Thus, the averaged carbon numbers of these 5 alkane QCs are determined
 118 as:

$$\left. \begin{aligned} \bar{n}_{(11-12)_{\text{alk}}} &= \left[\frac{\sum_{j=12}^{j=11} n_j X_j}{\sum_{j=12}^{j=11} X_j} \right] \\ \bar{n}_{(13-14)_{\text{alk}}} &= \left[\frac{\sum_{j=14}^{j=13} n_j X_j}{\sum_{j=14}^{j=13} X_j} \right] \\ \bar{n}_{(15-16)_{\text{alk}}} &= \left[\frac{\sum_{j=16}^{j=15} n_j X_j}{\sum_{j=16}^{j=15} X_j} \right] \\ \bar{n}_{(17-18)_{\text{alk}}} &= \left[\frac{\sum_{j=18}^{j=17} n_j X_j}{\sum_{j=18}^{j=17} X_j} \right] \\ \bar{n}_{(19-20)_{\text{alk}}} &= \left[\frac{\sum_{j=20}^{j=19} n_j X_j}{\sum_{j=20}^{j=19} X_j} \right] \end{aligned} \right\} \quad (6)$$

119 Similarly, if a certain group contains 11 components, these reduce to $N_i = \lceil 0.75 \times 11 \rceil = 8$. The first
 120 5 components remain unchanged, while the last 6 components form 3 QCs – distributed as 2
 121 components each, following the same procedure as shown in (6). The speed of change in mass
 122 fractions of certain species or groups is influenced by their high evaporation rates, which indicates
 123 the need to reduce their QC/C representation in the fuel composition. When the reduction in group
 124 mass fractions G_i is small (i.e. $\Delta G_i \leq K$), the code uses the previous number of QC/Cs, $N_{i_{old}}$ (i.e. $F =$
 125 1).



126
 127 Figure 1. Flowchart of the new algorithm, where the minimum change in mass fraction ratio $K =$
 128 0.1 , reduction factor $F = 0.75$ and the minimum ratio of droplet radii $\epsilon = 10^{-6}$.

129 In the new algorithm, users can define the minimum number of QC/Cs. This option is built into the
 130 final stage of the algorithm when further auto-reduction in the number of QC/Cs is blocked after this

131 number reaches a certain minimum value. For example, if the minimum number of QC/Cs is defined
 132 by the end-user as ‘10 QC/Cs’ and the remaining number of QC/Cs is ‘15’, the auto-reduction will lead
 133 to 11 QC/Cs ($[0.75 \times 15]$). However, the further reduction of 11 QC/Cs, following the algorithm,
 134 would lead to less than 10 QC/Cs. Hence, ‘11 QC/Cs’ will auto-reduce to ‘10 QC/Cs’ only.

135 The new algorithm can lead to a compromise between the accuracy of the DC model and the
 136 computational speed of the original MDQD model. The solution algorithm steps can be summarised
 137 as: 1) determine the input parameters for liquid and gas phases, 2) calculate thermodynamic and
 138 transport properties at each time-step, 3) update the molar fractions of individual species inside and
 139 at the surface of droplets, according to their partial pressures, 4) determine the temperature and
 140 mass fractions of species distributions inside the droplet, 5) determine the total evaporation rate and
 141 new droplet radius, 6) go to Step 1 if the ratio of droplet radius and the initial droplet radius is greater
 142 than an *a priori* chosen number $\varepsilon = 10^{-6}$; otherwise the droplet is assumed to have evaporated.

143 3. Heating and evaporation model

144 The discrete component (DC) model is used for the analysis of droplet heating and evaporation
 145 [26]. The Effective Thermal Conductivity (ETC) and Effective Diffusivity (ED) models are
 146 implemented in this model to take into account the effect of recirculation due to moving droplets
 147 [15,27]. The numerical algorithm used in our analysis is based on the analytical solutions to the
 148 transient heat conduction and species diffusion equations in the liquid phase, assuming that all
 149 processes are spherically symmetric. The following analytical solution for temperature $T = T(t, R)$ at
 150 the end of each time-step (t) was used [28]:

$$T(R, t) = \frac{R_d}{R} \sum_{n=1}^{\infty} \left\{ q_n \exp[-\kappa_R \lambda_n^2 t] - \frac{\sin \lambda_n}{\|v_n\|^2 \lambda_n^2} \mu_0(0) \exp[-\kappa_R \lambda_n^2 t] \right\} \sin \left(\lambda_n \frac{R}{R_d} \right) + T_{\text{eff}}(t), \quad (7)$$

151 where R is the distance from the centre of the droplet, t is time, $\|v_n\|^2 = \frac{1}{2} \left(1 + \frac{h_{0T}}{h_{0T}^2 + \lambda_n^2} \right)$, $q_n =$
 152 $\frac{1}{R_d \|v_n\|^2} \int_0^{R_d} \tilde{T}_0(R) \sin \left(\lambda_n \frac{R}{R_d} \right) dR$, $\tilde{T}_0(R) = R T_{d0}(R)/R_d$, $\kappa_R = \frac{k_{\text{eff}}}{c_l \rho_l R_d^2}$, $\mu_0(t) = \frac{h T_g(t) R_d}{k_{\text{eff}}}$, $h_{0T} = \left(\frac{h R_d}{k_{\text{eff}}} \right) -$
 153 1 , c_l is the liquid specific heat capacity and ρ_l is the density of liquid, the positive eigenvalues λ_n
 154 ($n > 0$) are determined from $\lambda \cos \lambda + h_{0T} \sin \lambda = 0$. The effective thermal conductivity k_{eff} is
 155 defined as:

$$k_{\text{eff}} = \chi k_l, \quad (8)$$

156 where k_l is the liquid thermal conductivity, and χ varies between 1 (when Peclet number $\text{Pe}_{d(l)} =$
 157 $\text{Re}_{d(l)} \text{Pr}_l < 10$) and 2.72 (for $\text{Pe}_{d(l)} > 500$). The model based on Expression (8) is known as the ETC
 158 model.

159 In Expression (7), the effect of droplet evaporation is accounted for using the effective
 160 temperature $T_{\text{eff}} = T_g + \frac{\rho_l L \dot{R}_{de}}{h}$, T_g is the ambient (gas) temperature, L is the latent heat of

161 evaporation, \dot{R}_{de} is the rate of change in droplet radius due to evaporation and $h = \text{Nu } k_g / 2R_d$ is the
 162 convective heat transfer coefficient, based on the Nusselt number (Nu) and the thermal conductivity
 163 of air (k_g).

164 The analytical solution to the equation for mass fractions of species i inside droplets was used
 165 [29]:

$$Y_{li} = \epsilon_i + \frac{1}{R} \left(\left[\exp \left[D_{\text{eff}} \left(\frac{\lambda_{0Y}}{R_d} \right)^2 t \right] [q_{i0} - \epsilon_i Q_0] \sinh \left(\lambda_{0Y} \frac{R}{R_d} \right) + \sum_{n=1}^{\infty} \left[\exp \left[-D_{\text{eff}} \left(\frac{\lambda_{nY}}{R_d} \right)^2 t \right] [q_{in} - \epsilon_i Q_n] \sin \left(\lambda_{nY} \frac{R}{R_d} \right) \right] \right) \right) \quad (9)$$

166 where $\epsilon_i = \frac{Y_{vis}}{\sum_i Y_{vis}}$, λ_{0Y} and λ_{nY} are calculated from $\tanh \lambda_{0Y} = -\lambda_{0Y} / h_{0Y}$ and $\tan \lambda_{nY} = -\lambda_{nY} / h_{0Y}$
 167 (for $n \geq 1$), respectively, $h_{0Y} = -\left(1 + \frac{\alpha R_d}{D_{\text{eff}}}\right)$, $\alpha = -\dot{m}_d / (4\pi\rho_l R_d^2)$,

$$Q_n = \begin{cases} -\frac{1}{\|v_{0Y}\|^2} \left(\frac{R_d}{\lambda_{0Y}} \right)^2 (1 + h_{0Y}) \sinh \lambda_{0Y} & \text{when } n = 0 \\ \frac{1}{\|v_{nY}\|^2} \left(\frac{R_d}{\lambda_{nY}} \right)^2 (1 + h_{0Y}) \sin \lambda_{nY} & \text{when } n \geq 1 \end{cases}, \quad (10)$$

$$q_{in} = \begin{cases} \frac{1}{\|v_{0Y}\|^2} \int_0^{R_d} R Y_{li0}(R) \sinh \left(\lambda_{0Y} \frac{R}{R_d} \right) dR & \text{when } n = 0 \\ \frac{1}{\|v_{nY}\|^2} \int_0^{R_d} R Y_{li0}(R) \sin \left(\lambda_{nY} \frac{R}{R_d} \right) dR & \text{when } n \geq 1 \end{cases} \quad (11)$$

168 $\|v_{0Y}\|^2 = -\frac{R_d}{2} \left(1 + \frac{h_{0Y}}{h_{0Y}^2 - \lambda_{0Y}^2}\right)$, $\|v_{nY}\|^2 = \frac{R_d}{2} \left(1 + \frac{h_{0Y}}{h_{0Y}^2 + \lambda_{nY}^2}\right)$ ($n \geq 1$), D_{eff} is the effective diffusivity,
 169 defined as:

$$D_{\text{eff}} = \chi_Y D_l, \quad (12)$$

170 D_l is the liquid diffusion coefficient, χ_Y is calculated as $\chi_Y = 1.86 +$
 171 $0.86 \tanh[2.225 \log_{10}(\text{Re}_{d(l)} \text{Sc}_l / 30)]$. The model based on Expression (12) is known as the ED
 172 model.

173 The droplet evaporation is calculated using the following expression:

$$\dot{m}_d = -2\pi R_d D_v \rho_{\text{total}} B_M \text{Sh}_{\text{iso}}, \quad (13)$$

174 where D_v is the binary diffusion coefficient of vapour in gas (air), $\rho_{\text{total}} = \rho_g + \rho_v$ is the total density
 175 of the mixture of vapour and ambient gas, Sh_{iso} is the Sherwood number for an isolated droplet in
 176 which the effects of droplet motion and evaporation are considered, using the Abramzon and
 177 Sirignano model [7], $B_M = \frac{Y_{vs} - Y_{\infty}}{1 - Y_{vs}}$ is the Spalding mass transfer number, and Y_{vs} and Y_{∞} are total
 178 vapour mass fractions in the vicinity of the droplet surface and in the far-field, respectively, $Y_{vs} =$
 179 $\sum_i Y_{vis}$, Y_{vis} are the vapour mass fractions of individual species i , calculated from the vapour molar
 180 fractions at the surface of droplet (X_{vis}), as:

$$X_{vis} = \gamma_i \frac{X_{is} p_{vis}^*}{p}, \quad (14)$$

181 where, X_{i_s} is the molar fraction of the i^{th} species at the surface of the droplet, γ_i is the activity
 182 coefficient of the i^{th} species, p_{vis}^* is the saturated pressure of individual species, and p is the ambient
 183 pressure. The DC model used in our analysis was verified in [30] and validated in [22,31]. Following
 184 [21,32], the activity coefficient was calculated, using the multi-component universal quasi-chemical
 185 functional group activity coefficients (UNIFAC) model [33,34].

186 4. Fuel composition

187 Diesel fuel, as described in [4], and gasoline fuel as used in advanced combustion engines – type C
 188 (FACE C), are used in our analysis to illustrate the efficiency of the new algorithm. The Diesel fuel
 189 used in [4] includes 98 hydrocarbon components, with the following groups and molar fractions:
 190 alkanes (40.0556%), cycloalkanes (14.8795%), bicycloalkanes (7.6154%), alkylbenzenes
 191 (16.1719%), indanes & tetralines (9.1537%), naphthalenes (8.6773%), tricycloalkanes (1.5647%,
 192 represented by the characteristic component $C_{19}H_{34}$), diaromatics (1.2240%, represented by the
 193 characteristic component $C_{13}H_{12}$), and phenanthrenes (0.6577%, represented by the characteristic
 194 component $C_{14}H_{10}$). The details of this composition are shown in Table 1.

195 Table 1. Molar fractions (%) of Diesel fuel components, excluding the characteristic components [4].

Carbon no	alkanes	cycloalkanes	bicycloalkanes	alkylbenzenes	indanes & tetralines	naphthalenes
C8	0.308	-	-	0.497	-	-
C9	3.032	-	-	3.2357	-	-
C10	5.0541	0.6408	0.6926	5.3584	1.3157	1.9366
C11	3.163	1.8745	1.0524	0.9492	1.3632	2.5290
C12	2.6156	1.6951	0.9753	1.9149	1.1951	1.4012
C13	2.5439	1.2646	0.6611	0.6873	1.0652	0.7692
C14	2.6497	1.3633	0.5631	0.6469	0.8406	0.4879
C15	3.1646	1.2353	0.4314	0.4782	0.7051	0.3843
C16	2.6579	1.0449	0.4921	0.4564	0.6684	0.2854
C17	2.8605	1.0162	0.6529	0.4204	0.5598	0.2072
C18	3.2403	1.2848	0.6554	0.5234	0.5357	0.2358
C19	3.5296	1.3566	0.9901	0.3226	0.3403	0.2151
C20	2.2338	0.9961	0.1965	0.2848	0.3227	0.2256
C21	1.443	0.5374	0.0935	0.2032	0.1638	-
C22	0.799	0.304	0.0701	0.0969	0.0781	-
C23	0.3972	0.109	0.0488	0.0494	-	-
C24	0.1903	0.0755	0.0234	0.0473	-	-
C25	0.0997	0.0445	0.0169	-	-	-
C26	0.0425	0.0214	-	-	-	-
C27	0.0309	0.0155	-	-	-	-
Total %	40.65	14.88	7.62	16.17	9.15	8.68

196 The composition of FACE C gasoline fuel is inferred from [23] and includes the following groups
 197 and molar fractions: n-alkanes (28.61%), iso-alkanes (65.19%), alkylbenzene (4.25%), indanes
 198 (0.10%, represented by its characteristic component C₉H₁₀), cycloalkanes (1.49%, represented by its
 199 characteristic component C₈H₁₆), and olefins (0.35%, represented by its characteristic component
 200 C₉H₁₈). The details of this composition are shown in Table 2.

201 Table 2. Molar fractions (%) of gasoline fuel components [23].

Carbon no	n-alkanes	iso-alkanes	alkylbenzenes	cycloalkanes	indanes	olefins
C4	3.905	0.092	-	-	-	-
C5	13.87	7.456	-	-	-	-
C6	10.842	2.98	-	-	-	-
C7	-	11.67	-	-	-	-
C8	-	42.17	0.242	1.49	-	-
C9	-	0.137	3.521	-	0.104	0.346
C10	0.01	0.36	0.44	-	-	-
C11	-	0.113	0.055	-	-	-
C12	0.012	-	-	-	-	-
Total%	28.64	64.98	4.26	1.49	0.104	0.346

202 Bioethanol free from water (anhydrous) is used in our study (described as ‘ethanol’) for the fuel
 203 mixtures. As in our previous study [22] we assume that ethanol is completely homogeneously spread
 204 in Diesel and gasoline fuel mixtures (this is a crude assumption where the mass fraction of
 205 ethanol/Diesel is high, due to the differences in their chemical characteristics and structures [35,36]).
 206 The following volume fractions of E85 (85% vol. ethanol and 15% vol. gasoline)/Diesel fuel blends
 207 are considered in this analysis: pure Diesel (98 hydrocarbons), E85-5 (5% vol. E85 and 95% vol.
 208 Diesel) (119 components, comprising 98 Diesel hydrocarbons, 20 gasoline hydrocarbons and 1
 209 ethanol), E85-20 (20% vol. E85 and 80% vol. Diesel) (119 components), E85-50 (50% vol. E85 and
 210 50% vol. Diesel) (119 components), and E85 (21 components, comprising 20 gasoline hydrocarbons
 211 and 1 ethanol). The thermodynamic and transport properties of gasoline, Diesel and ethanol are
 212 inferred from [4,22,23].

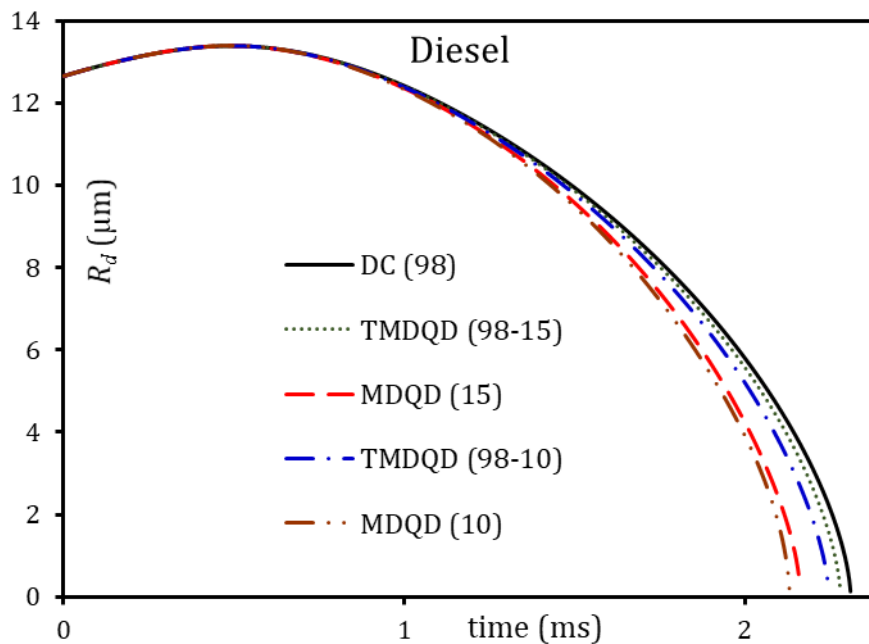
213 The liquid properties are calculated at the average droplet temperature ($T_{av} =$
 214 $\frac{3}{R_d^3} \int_0^{R_d} R^2 T(R) dR$). The vapour properties are calculated at the reference temperature ($T_r = \frac{2}{3} T_s +$
 215 $\frac{1}{3} T_g$). The density of gas (air) is calculated using the ideal gas law. The saturated vapour pressure and
 216 latent heat of evaporation are calculated at the droplet surface temperature T_s .

217 5. Results

218 The new algorithm was used for modelling the heating and evaporation of droplets of Diesel fuel
 219 and its E85 fuel blends. Following [21], the initial droplet diameter was taken equal to $d_o =$
 220 $25.32 \mu\text{m}$; the droplet velocity was assumed constant and equal to $U_d = 10 \text{ m. s}^{-1}$. The initial droplet

221 temperature was assumed equal to $T_0 = 298$ K. The ambient air pressure and temperature were
222 assumed to be constant and equal to $p_g = 30$ bar and $T_g = 800$ K, respectively.

223 The evolutions of pure Diesel fuel droplet surface temperatures and radii predicted using the DC
224 model, the original MDQD model and the new algorithm, are presented in Figures 2-3. Five cases are
225 shown: the contributions of all 98 components are considered, using the DC model (indicated as DC
226 (98)); the 98 components are reduced to 15 QC/Cs, using the original MDQD model (indicated as
227 MDQD (15)); the 98 components are reduced to 10 QC/Cs, using the original MDQD model (indicated
228 as MDQD (10)); the 98 components are auto-reduced to 15 (or 10) QC/Cs using the new algorithm
229 (indicated as TMDQD (98-15 (or 98-10))). The application of the TMDQD (98-15 (98-10)) led to 74
230 QC/Cs (i.e. the nearest integer to 98×0.75) at time instant 0.300 ms, 56 QC/Cs (i.e. $[74 \times 0.75]$) at
231 time-instant 0.450 ms, 42 QC/Cs (i.e. $[56 \times 0.75]$) at time-instant 0.599 ms, 32 QC/Cs (i.e.
232 $[0.75 \times 42]$) at time-instant 0.782 ms, 24 QC/Cs (i.e. $[0.75 \times 32]$) at time-instant 1.162 ms, 18 QC/Cs
233 (i.e. $[0.75 \times 24]$) at time-instant 1.687 ms, 15 QC/Cs at time-instant 1.887 ms and 10 QC/Cs at time-
234 instant 2.009 ms.

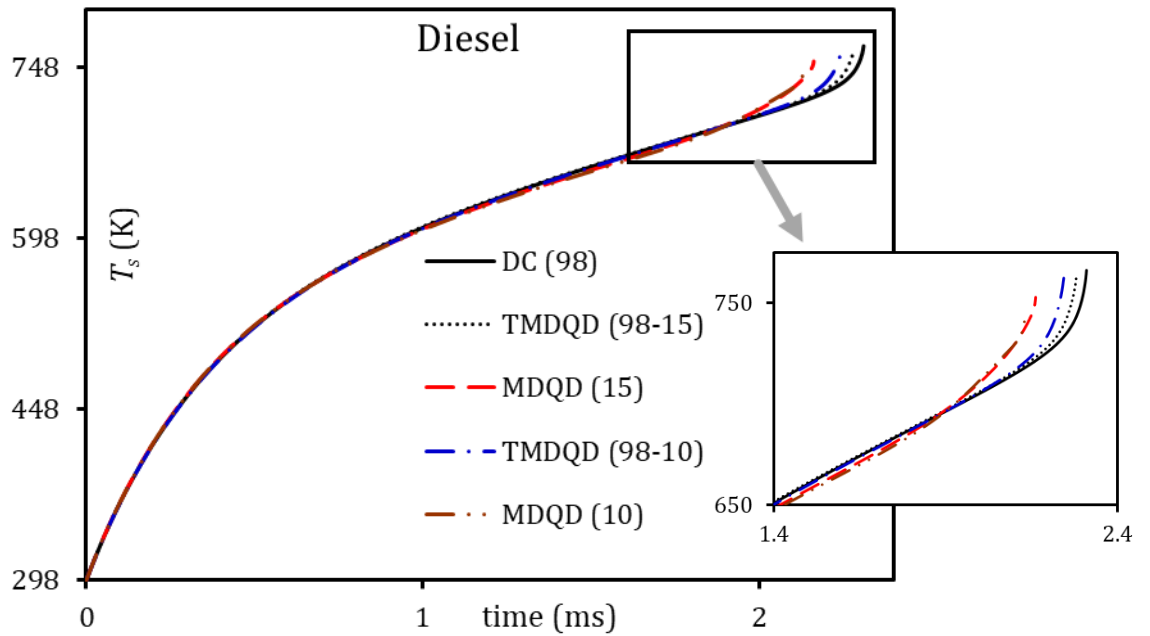


235
236 Figure 2. Evolutions of Diesel fuel (98 components) droplet radii versus time using the DC model, the
237 original MDQD model and the new algorithm (TMDQD).

238 As can be seen in Figure 2, TMDQD 98-15 shows droplet radius evolution and lifetime nearest to
239 those predicted using the DC model. This is followed by those predicted using TMDQD 98-10. The
240 same trends are observed for droplet surface temperatures (see Figure 3).

241 It can be seen from Figures 2 and 3 that the evolutions of Diesel droplet radii and surface
242 temperatures predicted using the new algorithm are almost identical to those predicted using the DC
243 model at the earlier stages of evaporation. This can be attributed to the fact that the TMDQD
244 algorithm starts with a higher number of QC/Cs (the full composition) compared with the

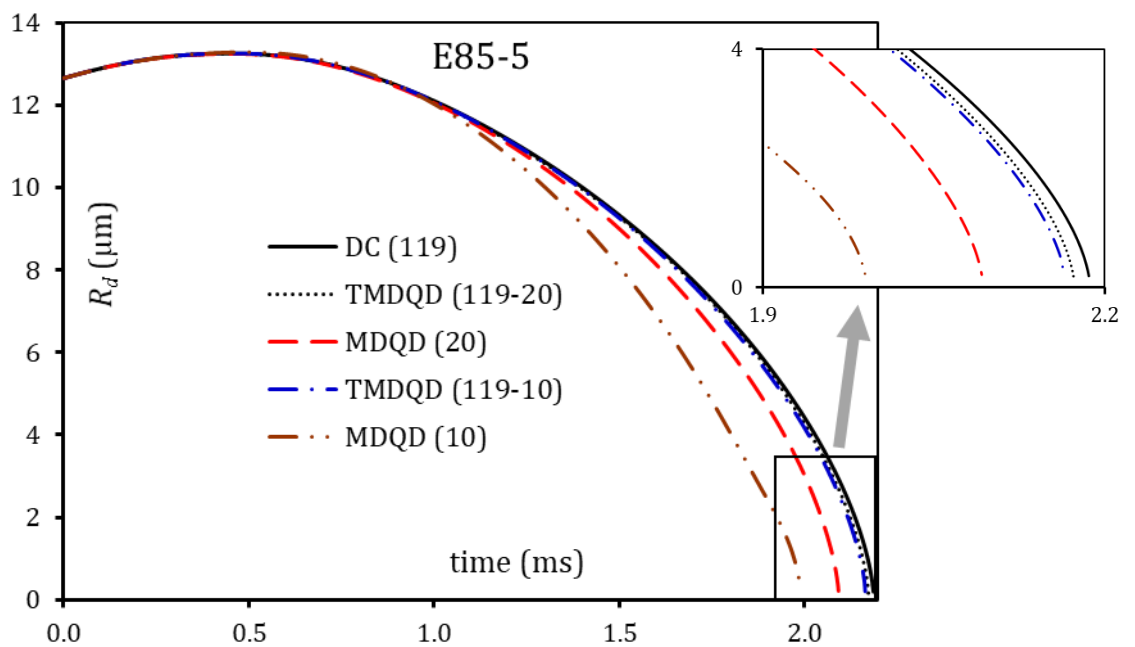
245 conventional MDQD model. The evolutions of blended Diesel-E85 fuel droplet radii and surface
246 temperatures were investigated accounting for the contributions of all 119 components of E85-5 fuel
247 blends, using the same algorithms as used for the plots in Figures 2 and 3. The results are presented
248 in Figures 4 and 5.



249

250

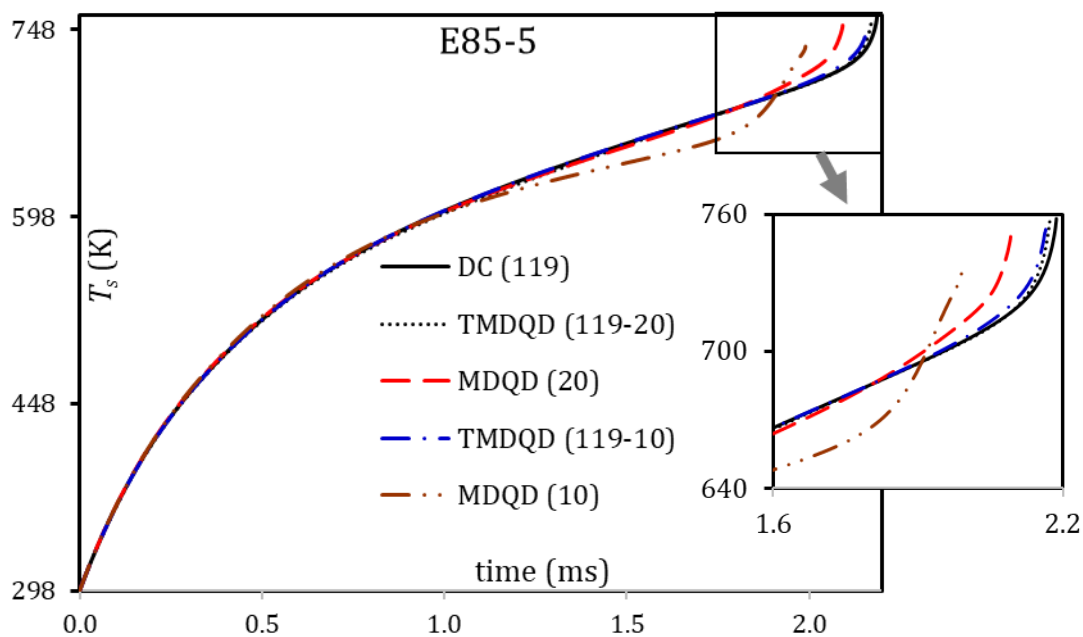
Figure 3. The same as Figure 2, but for droplet surface temperatures.



251

252

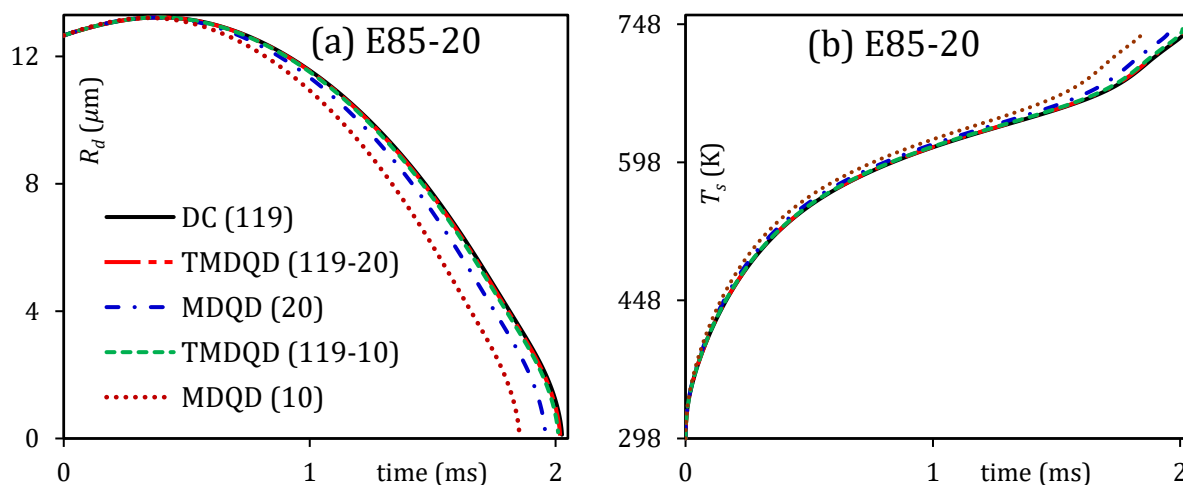
Figure 4. The same as Figure 2 but for E85-5 (95% Diesel and 5% E85) droplets.



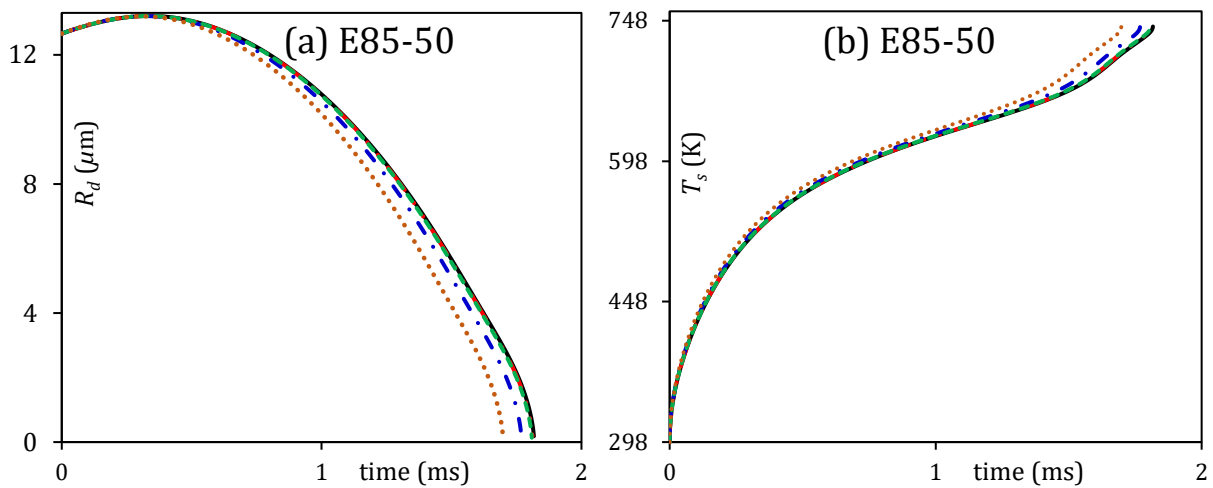
253
254

Figure 5. The same as Figure 3 but for E85-5 (95% Diesel and 5% E85) droplets.

255 As in the case of the pure Diesel fuel droplet (Figures 2 and 3), for the E85-5 fuel blend droplet,
 256 both the droplet lifetimes (Figure 4) and surface temperatures (Figure 5) predicted by the new
 257 algorithm are the closest to those predicted by the DC model. The predicted droplet lifetimes and
 258 evolutions of radii and surface temperatures of the other E85/Diesel fuel blends show the same
 259 trends as those presented in Figures 2–5. The predicted droplet lifetimes for several E85/Diesel fuel
 260 blends are presented in Table 3 and the corresponding plots are shown in Figures 6 and 7. In this
 261 table and these figures, the predictions of the original MDQD model, the new algorithm and the DC
 262 model are compared. An example of the detailed compositions of these blends, and the reduced
 263 components at various time instants is presented in Supplementary Material S1 for the E85-5 fuel
 264 blend.



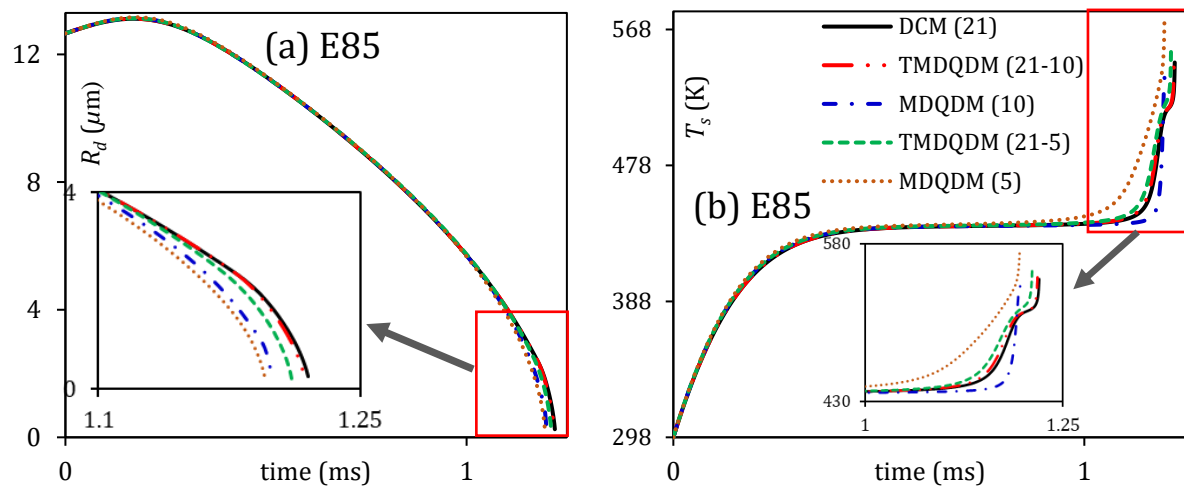
265



266

267

268 Figure 6. Evolutions of (a) droplet radii in μm and (b) surface temperatures in K versus time in ms
 269 for E85-20 and E85-50 fuel blends, using the DC (119 components), MDQD(20) (119 components are
 270 manually reduced to 20 QC/Cs), MDQD(10) (119 components are manually reduced to 10 QC/Cs),
 271 TMDQD(119-20) (119 components are auto-reduced to 20 QC/Cs), and TMDQD(119-10) (119
 272 components are auto-reduced to 10 QC/Cs).



273

274 Figure 7. The same as Figure 6, but for E85 using the DC (21 components), MDQD(10) (21
 275 components are manually reduced to 10 QC/Cs), MDQD(5) (21 components are manually reduced to
 276 5 QC/Cs), TMDQD(21-10) (21 components are auto-reduced to 10 QC/Cs), and TMDQD(21-5) (21
 277 components are auto-reduced to 5 QC/Cs).

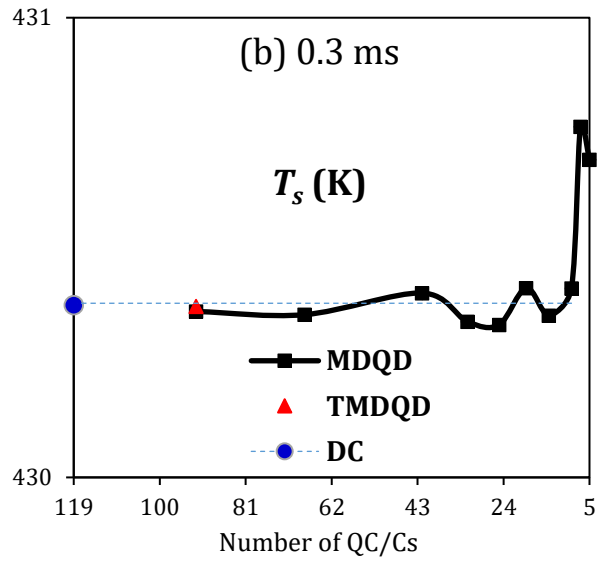
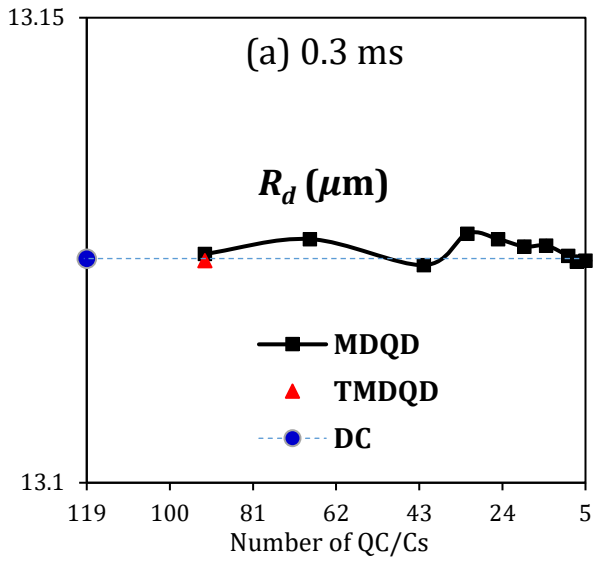
278 Table 3. Droplet lifetimes (ms) for Diesel (98 components), E85/Diesel blends (119 components) and
 279 E85 (21 components) fuels, predicted by the TMDQD algorithm and the original MDQD model for 20,
 280 10 and 5 QC/Cs. The errors in the predictions of TMDQD and MDQD are calculated relative to the

281 predictions of the DC model using parameter $\Delta\text{time} = (\text{time}_{\text{DC}} - \text{time}_{\text{model}}) \times 100\% / \text{time}_{\text{DC}}$, where
 282 time_{DC} is always greater than $\text{time}_{\text{model}}$.

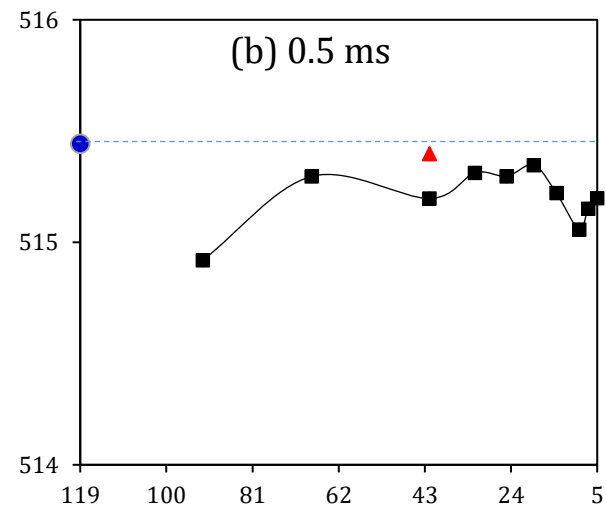
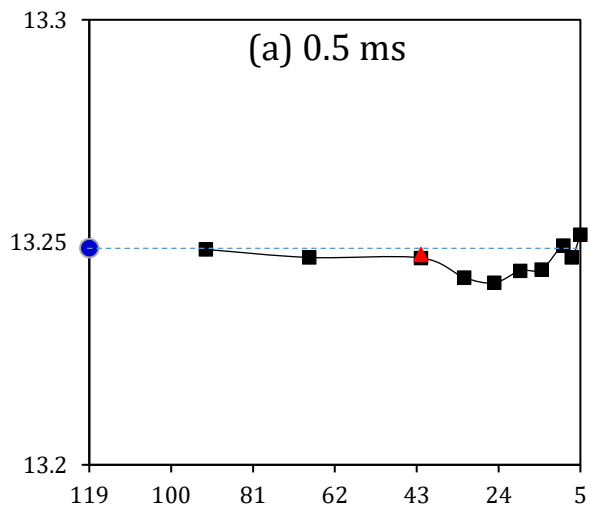
Model	Diesel	Δtime	E85-5	Δtime	E85-20	Δtime	E85-50	Δtime	E85	Δtime
DC	2.310	0	2.186	0	2.026	0	1.817	0	1.220	0
TMDQD(20)	2.280	1.3	2.173	0.4	2.018	0.4	1.812	0.3	-	-
MDQD(20)	2.160	6.4	2.092	4.1	1.960	3.4	1.769	2.6	-	-
TMDQD(10)	2.246	2.8	2.164	0.8	2.010	0.8	1.809	0.4	1.218	0.2
MDQD(10)	2.130	7.8	1.990	8.8	1.850	8.6	1.698	6.6	1.990	1.2
TMDQD(5)	2.217	4.0	2.144	1.9	1.998	1.4	1.799	1.0	1.211	0.7
MDQD(5)	1.985	14.1	1.888	13.6	1.839	9.2	1.681	7.5	1.195	2.1

283 As can be seen in Table 3, the errors of predictions made by the MDQD model and TMDQD
 284 algorithm in most cases decrease, and the droplet lifetimes become shorter when the ratios of
 285 E85/Diesel increase. The general trends indicate noticeable improvement in the predictions of
 286 droplet lifetimes using the TMDQD algorithm, compared to the original MDQD model with 20, 10 and
 287 5 QC/Cs. For example, reducing the 21 components of E85 fuel to 5 QC/Cs at the final stage of droplet
 288 evaporation, using this new algorithm, leads to underprediction of the droplet lifetime by up to 0.7%.
 289 In the case of the original MDQD model with 5 QC/Cs, this error increases to 2.1%. The processes
 290 preceding the onset of combustion (including physical autoignition delay) are typically 2–6 ms
 291 within the idle speed range of all IC engines [37,38]; this can be shorter (0.1 – 1.5 ms) for rapid
 292 compression Diesel engines [39]. With such a short time, the accuracy of prediction of droplet
 293 lifetimes becomes particularly important. Hence, the application of the new algorithm for simulating
 294 these processes can be recommended for such conditions.

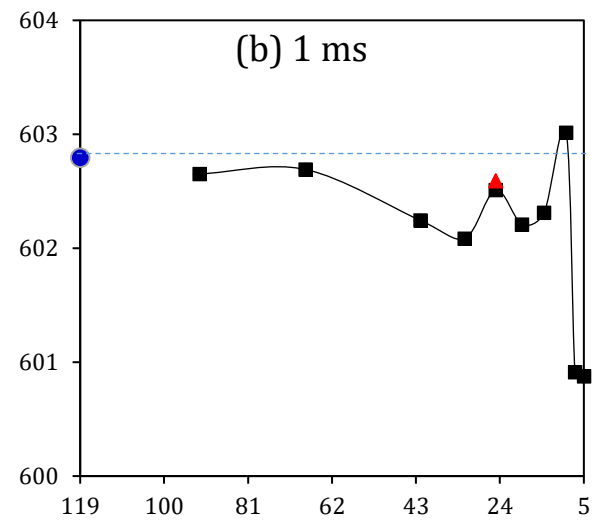
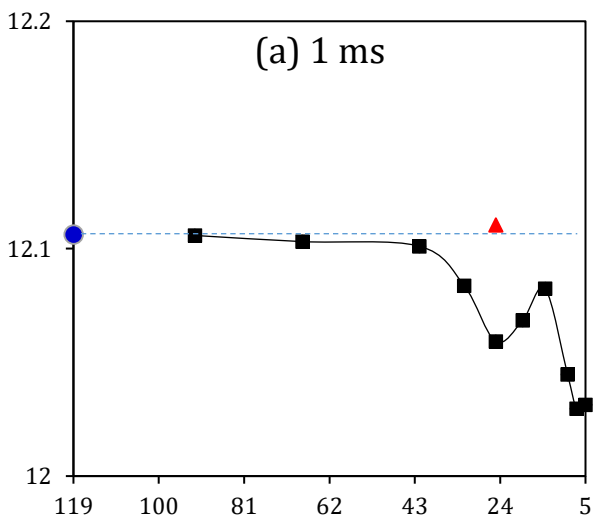
295 The values of droplet surface temperatures and radii versus the number of QC/Cs predicted using
 296 both versions of the MDQD based algorithms are shown in Figure 8. These results are estimated for
 297 the E85-5 fuel blend (inferred from [21,22]), composed of 119 components, at time instants $t = 0.3$
 298 ms, $t = 0.5$ ms, $t = 1$ ms, $t = 1.5$ ms and $t = 2$ ms. The values of the numbers of QC/Cs used by the
 299 TMDQD algorithm were fixed at these time instants and are shown as triangles. Note that in the
 300 TMDQD algorithm the full composition of fuel is auto-reduced to different numbers of QC/Cs at
 301 different time instants. In the case of the original MDQD model, the number of QC/Cs is pre-defined
 302 for each separate code run.



303

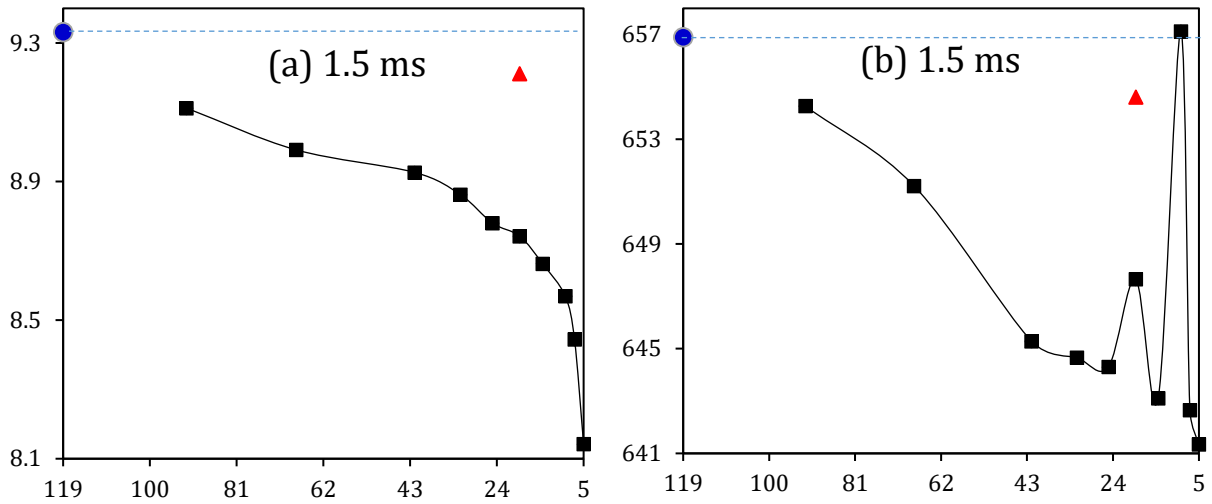


304

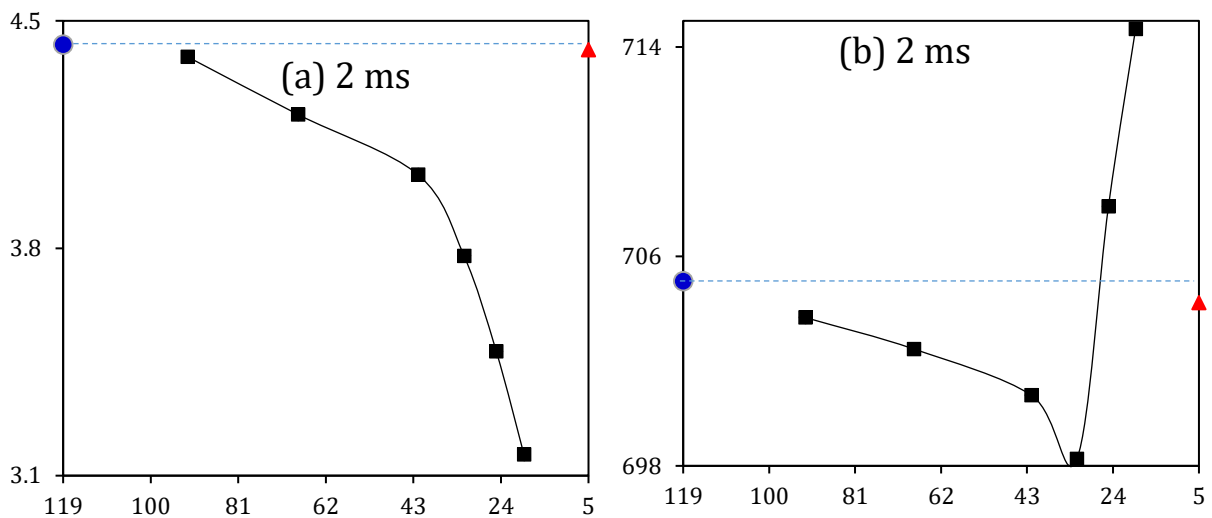


305

306



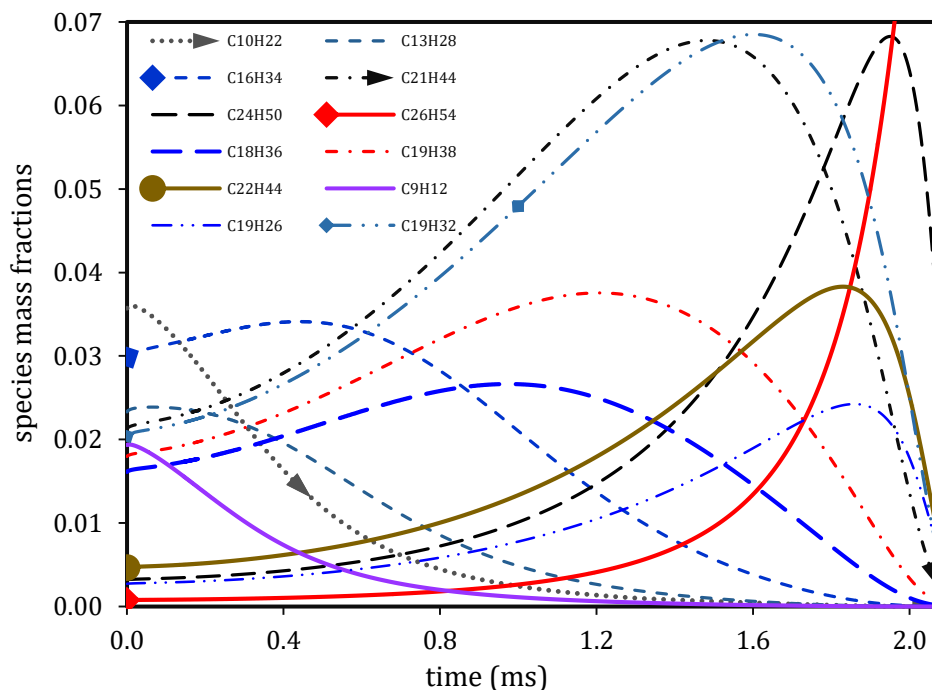
307



308 Figure 8. Droplet radii in μm (a) and surface temperatures in K (b) versus the numbers of QC/Cs
 309 predicted by the TMDQD algorithm (▲), the DC model (●) and the original MDQD model (■) at time
 310 instants (0.3 ms, 0.5 ms, 1 ms, 1.5 ms and 2 ms) for various numbers of QC/Cs, using the same
 311 parameters as in Figures 2-5.

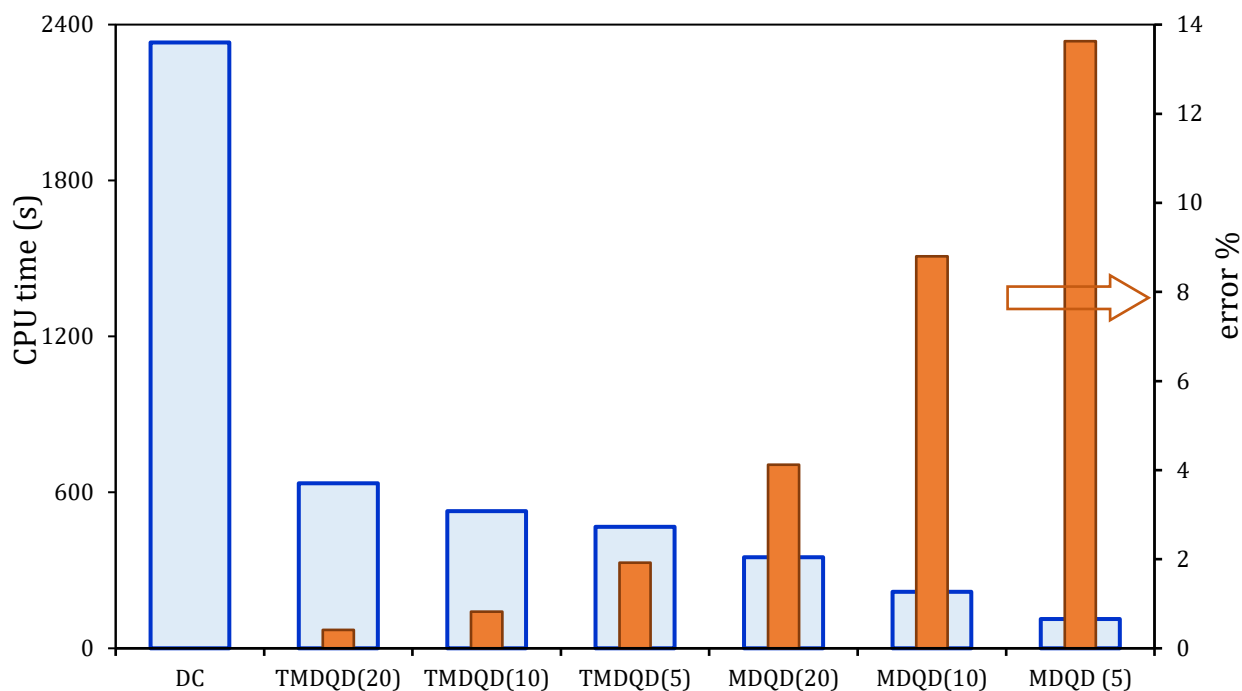
312 As can be seen from Figure 8, the predictions of the TMDQD algorithm for droplet surface
 313 temperatures and radii are generally more consistent with the DC model predictions than those
 314 predicted using the original MDQD model. Note that the predictions of both approaches are closer at
 315 the early stages of heating and evaporation (up to 0.5 ms) than at the later times. As in [4,20], the
 316 predictions of the original MDQD model show fluctuations in droplet radii and surface temperatures
 317 for small numbers of QC/Cs. This is attributed to the fact that the reduction in the number of QC/Cs
 318 in the original MDQD model is based on trial-and-error, which requires experienced end-users and
 319 makes it difficult to implement this approach into CFD codes. Note that the fluctuations predicted by
 320 the original MDQD model become less visible at later evaporation times (≥ 1 ms), when the lighter
 321 (volatile) components have mostly evaporated. At times close to the evaporation time (>1.5 ms), the
 322 original MDQD model fails to predict the droplet surface temperatures and radii accurately. The
 323 deviation becomes more noticeable for small numbers of QC/Cs in the MDQD.

324 The time evolution of mass fractions of selected species at the surface of an E85-5 fuel droplet,
325 predicted by the DC model, is shown in Figure 9. These are typical examples of the evolutions of
326 heavy, intermediate and light species of the initial 119 components in the E85-Diesel fuel blend.



327
328 Figure 9. Liquid mass fractions of species at the surface of an E85-5 fuel droplet versus time for the
329 same conditions as in Figures 4-7.

330 As follows from Figure 9, the evolutions of mass fractions of species at the surface of the droplet
331 show trends similar to those observed for Diesel, gasoline and biodiesel fuels [4,23]. The heavy
332 components ($C_{24}H_{50}$, $C_{26}H_{54}$) gradually dominate the droplet composition at the expense of the light
333 ones (C_9H_{12} , $C_{10}H_{22}$), while the intermediate species ($C_{16}H_{34}$, $C_{19}H_{38}$) first increase and then
334 decrease at later stages of droplet heating and evaporation. Also, the heavy species tend to evaporate
335 more slowly than the lighter ones, due to their lower saturation vapour pressures. The CPU times
336 required to run calculations and errors, using different models, for an E85-Diesel fuel blend are
337 presented in Figure 10 and Table 4.



338
 339 Figure 10. CPU times (wide bars) and errors (narrow bars) for six modelling approaches, compared
 340 with the predictions of the DC model for an E85-5 fuel blend. The errors are calculated as $\text{error}\% =$
 341 $(\text{time}_{\text{DC}} - \text{time}_{\text{model}}) \times 100\% / \text{time}_{\text{DC}}$, where time_{DC} is always greater than $\text{time}_{\text{model}}$. The full
 342 composition of an E85-5 fuel blend (119 components) is auto-reduced to 20, 10 and 5 QC/Cs using
 343 the TMDQD algorithm, indicated as TMDQD(20), TMDQD(10), TMDQD(5), respectively, and the same
 344 composition is reduced to 20, 10 and 5 QC/Cs using the original MDQD model, indicated as
 345 MDQD(20), MDQD(10) and MDQD(5), respectively.

346 Table 4. CPU time (in s) required for TDMDQ and MDQD model calculations for Diesel fuel or its
 347 blends (first columns), and the time saving compared to the DC model, calculated as $\text{T.S.}\% =$
 348 $(\text{CPU}_{\text{DC}} - \text{CPU}_{\text{model}}) \times 100\% / \text{CPU}_{\text{DC}}$ (second columns). The workstation used was fitted with an i7-
 349 3337U core, 4 GB RAM, and a 2.0 GHz processor. The time-step was set as 1 μs . An example of the
 350 detailed compositions of E85-5 during the reduction of QC/Cs predicted by TMDQD(5) is shown in
 351 Supplementary Material S1.

Model	CPU time (s) and time savings (T.S.%) compared to DCM									
	Diesel	T.S.%	E85-5	T.S.%	E85-20	T.S.%	E85-50	T.S.%	E85	T.S.%
DC	2511	-	2331	-	2177	-	1985	-	306	-
TMDQD(20)	789	68.6	635	72.8	537	75.3	488	75.42	-	-
MDQD(20)	428	82.9	351	84.9	427	80.4	363	81.71	-	-
TMDQD(10)	698	72.2	528	77.4	480	77.95	421	78.79	158	48.40
MDQD(10)	329	86.9	218	90.7	306	85.94	261	86.85	107	65.03
TMDQD(5)	621	75.3	467	80.0	472	78.32	396	80.03	141	53.92
MDQD (5)	140	94.4	113	95.2	110	94.9	103	94.80	79	74.18

352 As can be seen from Figure 10 and Table 4, there is a noticeable improvement in the predictions
 353 of the MDQD model with the new algorithm (TMDQD) compared to the same predictions made using
 354 the original MDQD model with fixed numbers of QC/Cs, but at the expense of computational time.

355 This is attributed to the fact that the new algorithm starts with higher numbers of QC/Cs than those
356 used in the original MDQD model. For example, the approximation of all 119 components of an E85-
357 5 fuel blend by 10 QC/Cs using the original MDQD model saves up to 90.7% of CPU time, and using
358 the TMDQD model saves up to 77.4% of CPU time. The approximation of the same blend by 5 QC/Cs
359 saves up to 95.2% and 80%, respectively, using the original MDQD and TMDQD models. The new
360 algorithm can be considered a compromise between the DC and MDQD models for wider engineering
361 applications where both accuracy and CPU efficiency are needed.

362 **6. Conclusion**

363 A new approach for calculating multi-component fuel droplet heating and evaporation based on
364 the previously developed multi-dimensional quasi-discrete (MDQD) model is suggested. As in the
365 original MDQD model, a large number of fuel components is reduced to a much smaller number of
366 components and quasi-components. In contrast to the original MDQD model, in the new approach
367 the number of quasi-components/components is not fixed during the whole process but is
368 automatically reduced when the droplet evaporates. The new approach is called the transient multi-
369 dimensional quasi-discrete (TMDQD) algorithm. This algorithm is applied to a wide range of E85
370 (85% ethanol and 15% gasoline) and Diesel fuel blends (E85, E85-5, E85-20, E85-50) and pure
371 Diesel.

372 It is shown that using the TMDQD algorithm allows us to reduce the full compositions of E85-
373 Diesel mixtures from their initial 119 components to 5 quasi-components/components at the end of
374 the heating and evaporation process with less than 1.9% errors in predicted droplet lifetimes and
375 temperatures. These predictions are shown to be more accurate than those obtained using the
376 original version of the MDQD model. The CPU time needed to run this algorithm is 80% less than that
377 needed by the Discrete Component (DC) model using the full composition of fuel.

378 **Acknowledgement**

379 The authors are grateful to the Institute for Future Transport and Cities, Coventry University, UK
380 (Project Ref. ECR019) (M.A., N.A.) and EPSRC, UK (Grant no. EP/M002608/1) (S.S.S.) for their
381 financial support.

References

- 382 [1] Wang J, Huang X, Qiao X, Ju D, Sun C. Experimental study on evaporation characteristics of single and
383 multiple fuel droplets. *J Energy Inst* 2020;93:1473–80. <https://doi.org/10.1016/j.joei.2020.01.009>.
- 384 [2] Sirignano WA. *Fluid Dynamics and Transport of Droplets and Sprays*. Cambridge, U.K: Cambridge
385 University Press; 1999.
- 386 [3] Divis M, Tiney NK, Lucas G. Spray Modeling of Multicomponent Fuels in Industrial Time Frames Using 3D
387 CFD. In: Liebl J, Beidl C, editors. *VPC – Simul. Test 2016*, Wiesbaden: Springer Fachmedien Wiesbaden;
388 2017, p. 132–52. https://doi.org/10.1007/978-3-658-16754-7_9.
- 389 [4] Sazhin SS, Al Qubeissi M, Nasiri R, Gun'ko VM, Elwardany AE, Lemoine F, et al. A multi-dimensional quasi-
390 discrete model for the analysis of Diesel fuel droplet heating and evaporation. *Fuel* 2014;129:238–66.
391 <https://doi.org/10.1016/j.fuel.2014.03.028>.
- 392 [5] Sazhin SS. *Droplets and Sprays*. London: Springer; 2014.

- 393 [6] Sazhin SS. Modelling of fuel droplet heating and evaporation: Recent results and unsolved problems. *Fuel*
394 2017;196:69–101. <https://doi.org/10.1016/j.fuel.2017.01.048>.
- 395 [7] Abramzon B, Sirignano WA. Droplet vaporization model for spray combustion calculations. *Int J Heat*
396 *Mass Transf* 1989;32:1605–18. [https://doi.org/10.1016/0017-9310\(89\)90043-4](https://doi.org/10.1016/0017-9310(89)90043-4).
- 397 [8] Al-Esawi N, Al Qubeissi M, Sazhin SS. The impact of fuel blends and ambient conditions on the heating
398 and evaporation of Diesel and biodiesel fuel droplets. *Int. Heat Transf. Conf. 16, Beijing, China:*
399 *Begellhouse*; 2018, p. 6641–8. <https://doi.org/10.1615/IHTC16.mpf.020772>.
- 400 [9] Castanet G, Frackowiak B, Tropea C, Lemoine F. Heat convection within evaporating droplets in strong
401 aerodynamic interactions. *Int J Heat Mass Transf* 2011;54:3267–76.
402 <https://doi.org/10.1016/j.ijheatmasstransfer.2011.03.060>.
- 403 [10] Saggese C, Singh AV, Xue X, Chu C, Kholghy MR, Zhang T, et al. The distillation curve and sooting
404 propensity of a typical jet fuel. *Fuel* 2019;235:350–62. <https://doi.org/10.1016/j.fuel.2018.07.099>.
- 405 [11] Kitano T, Nishio J, Kurose R, Komori S. Effects of ambient pressure, gas temperature and combustion
406 reaction on droplet evaporation. *Combust Flame* 2014;161:551–64.
407 <https://doi.org/10.1016/j.combustflame.2013.09.009>.
- 408 [12] Ali OM, Mamat R, Abdullah NR, Abdullah AA. Analysis of blended fuel properties and engine performance
409 with palm biodiesel–diesel blended fuel. *Renew Energy* 2016;86:59–67.
410 <https://doi.org/10.1016/j.renene.2015.07.103>.
- 411 [13] An H, Yang WM, Maghbouli A, Chou SK, Chua KJ. Detailed physical properties prediction of pure methyl
412 esters for biodiesel combustion modeling. *Appl Energy* 2013;102:647–56.
413 <https://doi.org/10.1016/j.apenergy.2012.08.009>.
- 414 [14] Sazhin SS, Al Qubeissi M, Xie J-F. Two approaches to modelling the heating of evaporating droplets. *Int*
415 *Commun Heat Mass Transf* 2014;57:353–6. <https://doi.org/10.1016/j.icheatmasstransfer.2014.08.004>.
- 416 [15] Sazhin SS, Al Qubeissi M, Kolodnytska R, Elwardany AE, Nasiri R, Heikal MR. Modelling of biodiesel fuel
417 droplet heating and evaporation. *Fuel* 2014;115:559–72. <https://doi.org/10.1016/j.fuel.2013.07.031>.
- 418 [16] Poulton L, Rybdylova O, Zubrilin IA, Matveev SG, Gurakov NI, Al Qubeissi M, et al. Modelling of multi-
419 component kerosene and surrogate fuel droplet heating and evaporation characteristics: A comparative
420 analysis. *Fuel* 2020;269:117115. <https://doi.org/10.1016/j.fuel.2020.117115>.
- 421 [17] Al-Esawi N, Al Qubeissi M, Kolodnytska R. The Impact of Biodiesel Fuel on Ethanol/Diesel Blends.
422 *Energies* 2019;12:1804. <https://doi.org/10.3390/en12091804>.
- 423 [18] Rybdylova O, Poulton L, Al Qubeissi M, Elwardany AE, Crua C, Khan T, et al. A model for multi-component
424 droplet heating and evaporation and its implementation into ANSYS Fluent. *Int Commun Heat Mass*
425 *Transf* 2018;90:29–33. <https://doi.org/10.1016/j.icheatmasstransfer.2017.10.018>.
- 426 [19] Sazhin SS, Elwardany AE, Sazhina EM, Heikal MR. A quasi-discrete model for heating and evaporation of
427 complex multicomponent hydrocarbon fuel droplets. *Int J Heat Mass Transf* 2011;54:4325–32.
428 <https://doi.org/10.1016/j.ijheatmasstransfer.2011.05.012>.
- 429 [20] Al Qubeissi M. Predictions of droplet heating and evaporation: an application to biodiesel, diesel, gasoline
430 and blended fuels. *Appl Therm Eng* 2018;136:260–7.
431 <https://doi.org/10.1016/j.applthermaleng.2018.03.010>.
- 432 [21] Al-Esawi N, Al Qubeissi M, Whitaker R, Sazhin SS. Blended E85–Diesel Fuel Droplet Heating and
433 Evaporation. *Energy Fuels* 2019;33:2477–88. <https://doi.org/10.1021/acs.energyfuels.8b03014>.
- 434 [22] Al Qubeissi M, Al-Esawi N, Sazhin SS, Ghaleeh M. Ethanol/Gasoline Droplet Heating and Evaporation:
435 Effects of Fuel Blends and Ambient Conditions. *Energy Fuels* 2018;32:6498–506.
436 <https://doi.org/10.1021/acs.energyfuels.8b00366>.
- 437 [23] Al Qubeissi M, Sazhin SS, Turner J, Begg S, Crua C, Heikal MR. Modelling of gasoline fuel droplets heating
438 and evaporation. *Fuel* 2015;159:373–84. <https://doi.org/10.1016/j.fuel.2015.06.028>.
- 439 [24] Al Qubeissi M, Sazhin SS, Elwardany AE. Modelling of blended Diesel and biodiesel fuel droplet heating
440 and evaporation. *Fuel* 2017;187:349–55. <https://doi.org/10.1016/j.fuel.2016.09.060>.
- 441 [25] Al-Esawi N, Al Qubeissi M. A new approach to formulation of complex fuel surrogates. *Fuel*
442 2021;283:118923. <https://doi.org/10.1016/j.fuel.2020.118923>.
- 443 [26] Sazhin SS. Advanced models of fuel droplet heating and evaporation. *Prog Energy Combust Sci*
444 2006;32:162–214. <https://doi.org/10.1016/j.pecs.2005.11.001>.
- 445 [27] Al Qubeissi M. Heating and Evaporation of Multi-Component Fuel Droplets. Stuttgart: WiSa; 2015.
- 446 [28] Sazhin SS, Krutitskii PA, Abdelghaffar WA, Sazhina EM, Mikhalovsky SV, Meikle ST, et al. Transient heating
447 of diesel fuel droplets. *Int J Heat Mass Transf* 2004;47:3327–40.
448 <https://doi.org/10.1016/j.ijheatmasstransfer.2004.01.011>.
- 449 [29] Sazhin SS, Elwardany A, Krutitskii PA, Castanet G, Lemoine F, Sazhina EM, et al. A simplified model for bi-
450 component droplet heating and evaporation. *Int J Heat Mass Transf* 2010;53:4495–505.
451 <https://doi.org/10.1016/j.ijheatmasstransfer.2010.06.044>.
- 452 [30] Elwardany AE, Gusev IG, Castanet G, Lemoine F, Sazhin SS. Mono- and multi-component droplet
453 cooling/heating and evaporation: comparative analysis of numerical models. *At Sprays* 2011;21:907–31.
454 <https://doi.org/10.1615/AtomizSpr.2012004194>.

- 455 [31] Sazhin SS, Elwardany AE, Krutitskii PA, Deprédurand V, Castanet G, Lemoine F, et al. Multi-component
456 droplet heating and evaporation: Numerical simulation versus experimental data. *Int J Therm Sci*
457 2011;50:1164–80. <https://doi.org/10.1016/j.ijthermalsci.2011.02.020>.
- 458 [32] Al-Esawi N, Al Qubeissi M, Sazhin SS, Whitaker R. The impacts of the activity coefficient on heating and
459 evaporation of ethanol/gasoline fuel blends. *Int Commun Heat Mass Transf* 2018;98:177–82.
460 <https://doi.org/10.1016/j.icheatmasstransfer.2018.08.018>.
- 461 [33] Poling BE, Prausnitz JM, O'Connell JP. *The properties of gases and liquids*. New York: McGraw-Hill; 2001.
- 462 [34] Reid RC, Prausnitz JM, Poling BE. *The properties of gases and liquids*. 4th ed. New York: McGraw-Hill;
463 1987.
- 464 [35] Kwanchareon P, Luengnaruemitchai A, Jai-In S. Solubility of a diesel–biodiesel–ethanol blend, its fuel
465 properties, and its emission characteristics from diesel engine. *Fuel* 2007;86:1053–61.
466 <https://doi.org/10.1016/j.fuel.2006.09.034>.
- 467 [36] Satgé de Caro P. Interest of combining an additive with diesel–ethanol blends for use in diesel engines.
468 *Fuel* 2001;80:565–74. [https://doi.org/10.1016/S0016-2361\(00\)00117-4](https://doi.org/10.1016/S0016-2361(00)00117-4).
- 469 [37] Efthymiou P, Davy MH, Garner CP, Hargrave GK, Rimmer JET, Richardson D, et al. An optical investigation
470 of a cold-start DISI engine startup strategy. *Intern. Combust. Engines Perform. Fuel Econ. Emiss., Elsevier*;
471 2013, p. 33–52. <https://doi.org/10.1533/9781782421849.1.33>.
- 472 [38] Petrukhin NV, Grishin NN, Sergeev SM. Ignition Delay Time – an Important Fuel Property. *Chem Technol*
473 *Fuels Oils* 2016;51:581–4. <https://doi.org/10.1007/s10553-016-0642-0>.
- 474 [39] Kobori S, Kamimoto T, Aradi AA. A study of ignition delay of diesel fuel sprays. *Int J Engine Res* 2000;1:29–
475 39. <https://doi.org/10.1243/1468087001545245>.